Editors' Suggestion

Temperature gradient driven motion of magnetic domains in a magnetic metal multilayer by entropic forces

Lin Huang [1,2,*] Joseph Barker [1] Lekshmi Kailas [1] Soumyarup Hait [1] Simon D. Connell [1] Gavin Burnell [1] and Christopher H. Marrows [1,†]

[1]*School of Physics and Astronomy, University of Leeds, Leeds LS2 9JT, United Kingdom*

[2]*School of Material Science, University of Sheffield, Sheffield S10 2TN, United Kingdom*

(Received 18 June 2025; revised 13 November 2025; accepted 5 December 2025; published 20 January 2026)

We studied the displacement of magnetic domains under temperature gradients in perpendicularly magnetized $Ta/[Pt/Co_{68}B_{32}/Ir]_{\times 10}/Pt$ multilayer tracks with microfabricated Pt heaters and thermometers by magnetic force microscopy. Subtracting out the effects of the Oersted field from the heating current reveals the pure temperature gradient driven motion, which is always toward the heater. The higher the thermal gradient along the track is (owing to the proximity to the heater or larger heater currents), the greater the observed displacements of the domains are, up to a velocity of around 1 nm/s in a temperature gradient of 20 K/μm. This velocity lies in the creep regime. Quantitative estimates of the strength of different driving mechanisms for the effect that have been proposed theoretically show that entropic forces dominate over those arising from the spin Seebeck and spin-dependent Seebeck effects in driving the domain motion.

DOI: 10.1103/152r-5wvt

I. INTRODUCTION

The field of spin caloritronics [1–4] lies at the intersection of thermoelectric effects and spintronics. Although it is well-known that the dynamics of spin textures such as domain walls (DWs) [5–7] and skyrmions [8–11] can be driven by the flow of currents down electrical potential gradients, spin caloritronics opens up the possibility that motion can be driven by temperature gradients ∇T.

Three principal mechanisms are proposed for this. First, in the spin Seebeck effect [12–14] a current of magnons flows down a temperature gradient. This can take place in an insulator or metal, and the current of angular momentum can exert a spin transfer torque (STT) on a spin texture [15–22]. Second, the spin-dependent Seebeck effect takes place in metals, in which a pure spin current of electrons flows down the temperature gradient [23,24]. Again, this spin current can exert spin-transfer torques on spin textures [25]. Third, entropic forces arise due to the gradient of temperature-dependent magnetic parameters such as magnetization M_{sat} and exchange stiffness A, which determine the energy of the spin texture [26]. Although atomistic simulations of a DW in an Fe monolayer on W using a Landau-Lifshitz-Gilbert approach were interpreted only in terms of magnon current flows [27], micromagnetic simulations of a permalloy wire using the Landau-Lifschitz-Bloch equation suggest that these entropic effects are likely to be the predominant driving force for DW motion [28].

Experimentally, early evidence of thermal STTs included the current dependence of switching fields [29] and the increased likelihood of finding a DW in a spot in the sample heated by a laser [30–32]. Analysis of the mechanism at play was limited or of a qualitative nature. DW motion has been directly imaged in an yttrium iron garnet film using the magneto-optical Kerr effect and was interpreted purely in terms of magnon currents [33]. The unidirectional component of DW motion under a current pulse in a (metallic) permalloy wire has also been interpreted in terms of the magnon spin transfer picture [34]. In all of these experiments, the DW moves toward the hot region. For skyrmions, the picture is less clear. The motion of a skyrmion lattice toward hotter regions has been observed in Cu_2OSeO_3 [35], but it is toward colder regions in $[Pt/CoFeB/Ta]_{15}$ multilayers [36]. This discrepancy motivated the work of Raimondo *et al.* in the theoretical study of how different temperature scalings of the magnetic free energy terms lead to entropic forces [37].

In this paper, we report a study of domain motion in a perpendicularly magnetized Pt/CoB/Ir metal multilayer driven by a temperature gradient. Our principal experimental result is that the domains always move toward the hotter region once a critical value of the temperature gradient is exceeded. We observe larger displacements of the domains closer to the heater, where ∇T is larger, allowing us to map the temperature profile. Estimates of the strength of the different driving forces that lead to domain motion, based on our experimentally measured parameters, indicate that motion driven by entropic forces dominates over spin transfer torques arising

*Present address: CORNERSTONE, Optoelectronics Research Centre, University of Southampton, Building 60, University Road, Southampton SO17 1BJ, United Kingdom.

†Contact author: c.h.marrows@leeds.ac.uk

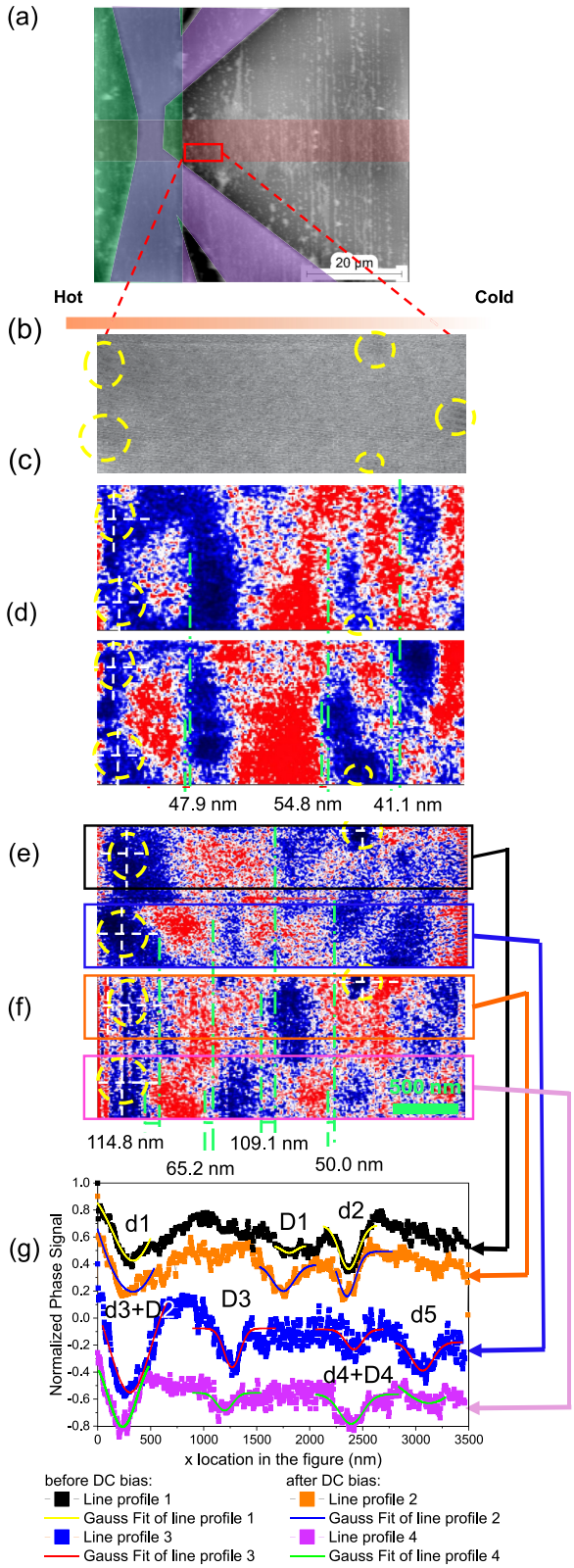

FIG. 1. MFM imaging of thermally induced domain motion. (a) Optical micrograph of the magnetic track (red) spanned by an electrically isolated (green) Pt heater and thermometer (purple). (b) MFM image when the track is fully saturated at +700 Oe, showing defect positions by dashed yellow circles. (c) and (d) MFM images at +30 Oe before and after a +30 mA current was applied to the heater, respectively. (e) and (f) MFM images at +30 Oe before and after a −30 mA current was applied to the heater, respectively. Dashed green lines indicate the position of the leading edge of the reverse domains. The colored boxes indicate the 50 pixel wide strips that were integrated to yield the line profiles that are shown in (g), offset for clarity. Gaussian fits to the line profile dips (marked "D" for a domain and "d" for a defect) are indicated by the solid colored lines.

from currents of both magnons and electrons, confirming the prediction of Moretti *et al.* [28].

II. EXPERIMENT

A false-color image of our sample is shown in Fig. 1(a). The 10 μm wide magnetic track (red region) was patterned from a Ta(20 Å)/[Pt(7 Å)/$Co_{68}B_{32}$(8 Å)/Ir(5 Å)]$_{\times 10}$/Pt(14 Å) multilayer that is perpendicularly magnetized. The track was partly covered by 100 nm of insulating SiO_x (green region) to electrically isolate it from a 250 nm thick Pt heater and thermometer wire (purple region). The SiO_x was deposited by rf sputtering, and the metals were deposited by dc sputtering. All patterning was performed by conventional photolithography. In the Supplemental Material [38] (which includes Refs. [39, 40]) we show a hysteresis loop of a sheet film of equivalent material that confirms perpendicular magnetization, along with typical domain patterns.

We used magnetic force microscopy (MFM) to observe the magnetic domains and their motion under magnetic fields H applied perpendicular to the sample plane. Figure 1(b) shows an MFM image acquired at $H = +700$ Oe, strong enough to magnetically saturate the track. The region of the track imaged here is indicated by the red box in Fig. 1(a). In this saturated state, ideally, the magnetic contrast must be uniform. Therefore, we can identify five patches of contrast as defects, which are marked by the dashed yellow circles. We used these defects as reference points for measuring the motion of magnetic domains.

Figure 1(c) shows an MFM image after saturation at +600 Oe acquired at $H = +30$ Oe, where regions of blue contrast corresponding to reverse domains are evident. Drift in the MFM imaging of the measured area reduces the number of defects we can resolve, but the same area can still be identified. Figure 1(d) shows the same area after passing a +30 mA current I through the heater for 2 min while holding H constant at +30 Oe. This generates a temperature gradient down the track, as indicated above Fig. 1(b). The dashed green lines indicate the motion of the leading edges of the domains toward the heater by a few tens of nanometers.

The domains were erased and renucleated by saturating the sample at $H > 700$ Oe and then decreasing H back to +30 Oe. The domains often reappear in broadly similar positions [Fig. 1(e)]. We again applied a current to the Pt heater, but this time with a negative current $I = -30$ mA. Figure 1(f) shows that a negative current also drives the domains toward the heater, this time by several tens of nanometers over 2 min.

To quantify the domain motion, we generated line profiles through the domains by integrating 50 pixel wide strips (corresponding to 570 nm). Examples are shown in Fig. 1(g). The dips in the line profiles correspond to the contrast from

both domains that are mobile (labeled "D") and the previously identified defect positions (labeled "d"). We aligned the images using the defect positions and fitted Gaussians to the most prominent dips, shown by solid lines. The centers of the fitted Gaussians are taken as the positions of the different features. As expected, we do not see motion outside the fitting uncertainty for the defects. We take the change in position of a domain to be its displacement under the effect of ∇T during the 120 s that the heater current flows. Taking the domain motion between the black and orange line profiles as an example, which moved -120 ± 30 nm, this yields an average velocity of $v \approx -0.9 \pm 0.2$ nm/s. (Motion toward the heater is in the negative x direction.) A table giving all of the fitting parameters for the line profiles shown in Fig. 1(g) is presented in the Supplemental Material [38].

We find that the domains always move toward the hotter region, but their average velocity while the heater current I flows depends on its direction, as in the example shown in Fig. 1. An explanation of this difference is that it is due to the Oersted field generated by I. This field will be vertical where it passes through the magnetic track and will become weaker with distance from the Pt heater according to the Biot-Savart law. The sign of I determines the sign of this field and its gradient, which can enhance or diminish any effect on the motion of the domain due to ∇T. We discuss this point in more detail in the Supplemental Material [38]. In our experiments the domain wall always moves toward the heater, so the net force in this direction must always be larger there than any opposing effect from the Oersted field. The displacement is indeed larger for $I < 0$ and smaller for $I > 0$ for positive H, consistent with our observations.

We confirmed the effect on the Oersted field from the heater wire on the domains by renucleation with opposite field H. This will cause the Oersted field forces to invert. In Fig. 2(a), we show data for a variety of domains at different distances from the heater and for different combinations of I and H. As before, $I = \pm 30$ mA, $H = \pm 30$ Oe, and the current was applied for 2 min. Although the domains always move toward the heater, they consistently move further when the Oersted field gradient gives rise to an attractive force (H and I have opposite signs; blue dashed line) and less far when the force is repulsive (H and I have the same sign; red dashed line).

Although so far we have implicitly described the domains as rigid objects, they are, of course, regions of reverse magnetization between two domain walls, and it is, in fact, these walls upon which temperature gradients will act. We can see from the data in Fig. 2(a) that the domains move at significantly higher average speeds if they are closer to the heater, implying that the temperature gradient is steeper there. This means that there will be a small difference in the magnitude of ∇T for the walls on either side of each domain. Given the $1/x$ dependence of the Oersted field, its gradient will also be slightly different for each of the two walls. By examining the widths of the fitted Gaussians we can hence study any domain expansion or contraction that arises from differential domain wall movement on either side of the domain. The results are shown in Fig. 2(b), where Δd_{d} is the change in domain size. The data show that the domains expand when I and H have opposite signs and contract when they have the same sign. Again, the effects are stronger when the domains are closer to the heater, where the gradients are stronger. These results are consistent with the force model shown in Fig. S3 in the Supplemental Material [38] and thus further support this picture.

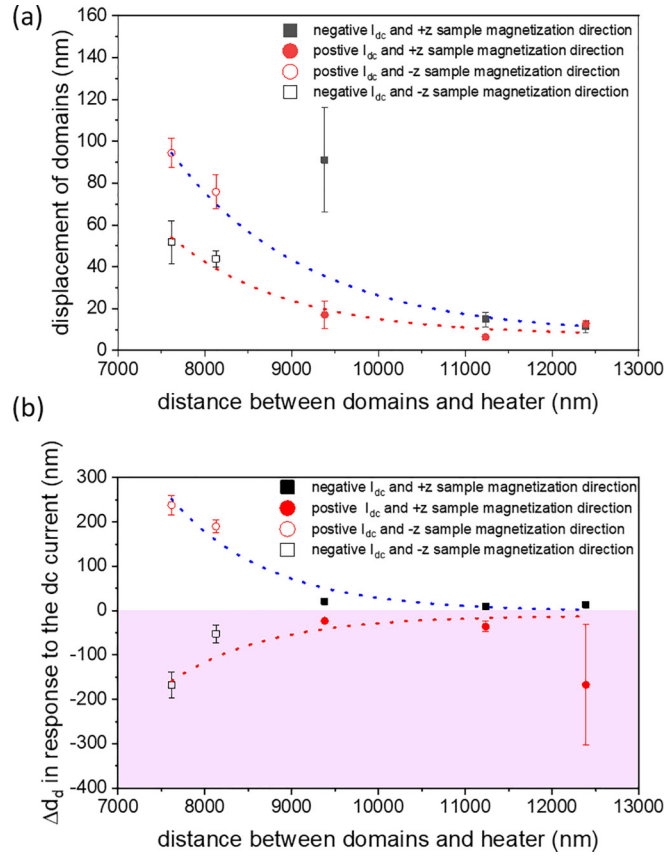

FIG. 2. Effects of the changing sign of I and H. (a) Domain motion and (b) expansion and contraction. The domains were driven by heater currents $I = \pm 30$ mA for both magnetization directions stabilized in fields $H = \pm 30$ Oe. Dashed lines are guides to the eye that link related datasets. In (a), the blue (red) dashed line represents domain displacement when the choice of the combination of I and H leads to an Oersted field gradient that assists (opposes) the motion toward the heated region. In (b), the blue and red dashed lines indicate the effect on the domain size.

In order to extract the motion arising only from ∇T, we average the measurements for a given renucleated domain for both positive and negative heater currents, which will cancel out the Oersted field gradient induced contribution to the motion. The resulting relationship between the ∇T induced domain displacement and distance from the heater is shown in Fig. 3(a) for a range of heater currents between 20 and 50 mA. The abscissa shows the distance from the domain to the heater, and the error bar is the standard deviation of the positions of four different domains after every pulse (three repeat pulses for each condition). The ordinate shows the domain displacement, and the error bar is the standard deviation of the displacement of domains after every pulse. There is considerable variation in the data caused by sample nonuniformities. Nevertheless, the main trends are clear. For $I = 20$ mA we observed no displacement to within the uncertainty

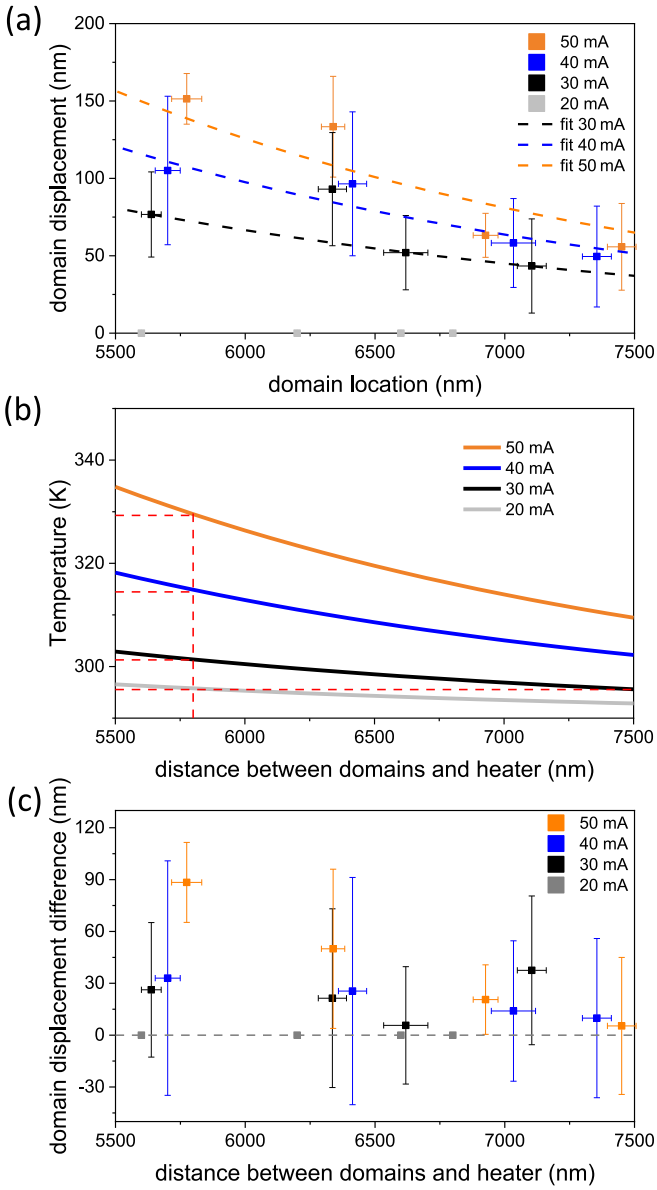

FIG. 3. Temperature gradient driven domain motion. (a) Average of the domain displacement after cancellation of Oersted field effects. (b) Estimated temperature profiles along the magnetic track. The red dashed lines point out the different temperatures at $x = 5800$ nm, the position of a defect, generated by different dc currents. (c) The difference in the displacement of the domain driven by varying positive and negative currents.

of our measurement. Motion sets in when the current is 30 mA or higher, and larger displacements are observed when the current rises further.

As in Fig. 2, another clear trend in Fig. 3 is that larger displacements (faster motion) are observed for domains close to the heater. This implies that the temperature gradient is steeper there. A simple assumption is that temperature varies exponentially with position x along the track as heat conducts away into the substrate, which we can quantify as

$$T(x) = T_{\text{lab}} + \Delta T \exp\left(-\frac{x}{l_{\text{T}}}\right), \tag{1}$$

where $x = 0$ is the edge of the heater wire, $T_{\text{lab}} = 290$ K is the laboratory ambient temperature, ΔT is the temperature rise for the heater wire taken from the Pt heater calibration (see Supplemental Material [38]), and l_{T} is the characteristic length scale for a $1/e$ decay of the temperature. Differentiating yields $\nabla T = -(\Delta T/l_{\text{T}})\exp(-x/l_{\text{T}})$. We then define the thermal efficiency k in terms of the average domain displacement $\Delta x_{\text{d}} = k\nabla T$ since DW velocity is expected to be proportional to ∇T [27]. We fitted this expression to our data as shown in Fig. 3(a) to obtain $k = 4700 \pm 600$ nm^{2}K^{-1} and $l_{\text{T}} = 2400 \pm 200$ nm. These values were then used to construct the $T(x)$ profiles shown in Fig. 3(b) from Eq. (1).

For our highest current, $I = 50$ mA, the temperature at the position of a prominent defect—$x = 5800$ nm, marked by a red dashed line—was lower than 330 K. Thus, we can say that the region imaged here by MFM remained well below the Curie temperature since we can still observe the magnetic pattern, and structural changes to the multilayer are also unlikely for these modest temperature increases. Moreover, $\nabla T = -2.4$ K/μm at $x = 5800$ nm generated by 20 mA (no motion) is just below $\nabla T = -2.6$ K/μm generated by 30 mA current at $x = 7200$ nm (slowest motion observed). The threshold temperature gradient for the onset of motion in our system therefore lies between these two values, $\nabla T_{\text{threshold}} = -2.5 \pm 0.1$ K/μm.

In Fig. 2(c), we plot the difference in domain displacement for positive and negative I, which is a measure of the strength of the Oersted field gradient, which we might expect to go as $\partial H/\partial x \sim -x^{-2}$ by differentiating the Biot-Savart law. Although the error bars on the data are too large to fit the data to this form precisely, the expected broad trend that the difference in displacements is larger closer to the current-carrying wire and when I is larger can be seen in the data.

The order of magnitude of the effect we find is an average velocity ~ -1 nm/s in a temperature gradient of ~ -20 K/μm—very slow and hence expected to be in the creep regime [41]. (Negative velocity indicates motion toward the heater, the edge of which is at $x = 0$.)

III. DISCUSSION

We estimate the strengths of different mechanisms that can contribute to this ∇T driven domain motion. In each case we use existing models that yield the velocity in the viscous flow regime. Since DWs exhibit Galilean dynamics where the velocity is proportional to the driving force [5,42,43], we take the relative sizes of these velocities to be representative of the relative sizes of the driving forces, which will also be responsible for any creep motion.

A. Magnon currents

For the spin Seebeck effect, we follow the method of Jiang *et al.* [33], who wrote the velocity of a domain wall under a current density J_{m} of magnons as

$$v = -\frac{\beta}{\alpha}\frac{\gamma\hbar}{M_{\text{s}}}J_{\text{m}}, \tag{2}$$

where $\gamma = 1.76 \times 10^{11}$ Hz/T is the gyromagnetic ratio. A typical value for the Gilbert damping in such a multilayer

is $\alpha \approx 0.07$ [11], and since the nonadiabaticity parameter β is essentially unknown but typically of the same order of magnitude, we set $\beta = \alpha$ since they are likely to be of the same order of magnitude. We use a value of $M_s = 532$ kA/m for the saturation magnetization of CoB at ~325 K based on our superconducting quantum interference device vibrating-sample magnetometer (SQUID-VSM) measurements.

The formula given in Ref. [33] for the magnon current density is

$$J_m = -\frac{k_B \nabla T}{6\pi^2 \lambda \hbar \alpha} F_0, \tag{3}$$

in which "$F_0 \approx 1$ is a coefficient arising in the kinetic theory of magnonic STT." The remaining material parameter to be determined is the thermal magnon wavelength λ. We estimate it using [44]

$$\lambda = \sqrt{\frac{D_0}{k_B T}}, \tag{4}$$

where $D_0 = 5.65 \times 10^{-40}\,\mathrm{J/m^2}$ is the spin wave exchange stiffness, determined from a fit to the SQUID-VSM data for our film (see [38]). This value yields $\lambda = 0.36$ nm at $T = 325$ K.

Inserting this value for λ into Eq. (S3) yields $J_m = 1.8 \times 10^{27}\,\mathrm{m^{-2}\,s^{-1}}$ for $\nabla T = -20$ K/μm. (Typical electron current densities for STT are $\sim 10^{12}\,\mathrm{A/m^2}$, which corresponds to a particle flux density of $\sim 6 \times 10^{30}\,\mathrm{m^{-2}\,s^{-1}}$.)

Putting this value for J_m into Eq. (2) leads to $v = -6.2$ cm/s. This value agrees in sign with the experimental observation but is many orders of magnitude larger. This is, perhaps, not surprising since the expressions above assume a viscous flow regime, whereas the experiment is in the creep regime. Nevertheless, this value can act as a measure of the strength of the STT arising from the magnon current with respect to other mechanisms.

B. Electronic pure spin currents

For a conventional electrical charge current density J_c, the velocity of a DW driven by STT is usually written as [5,7,33]

$$v = -\frac{\beta}{\alpha}\frac{\gamma \hbar P}{2eM_s} J_c, \tag{5}$$

where $P = (\sigma_\uparrow - \sigma_\downarrow)/(\sigma_\uparrow + \sigma_\downarrow)$ is the spin polarization of the current; typically, $P \sim 0.5$ in the diffusive regime in Co [45]. The minus sign ensures that the domain wall velocity is in the direction of electron flow [43]. Since the spin current $J_s = PJ_e$, we can rewrite this as

$$v = -\frac{\beta}{\alpha}\frac{\gamma \hbar}{2eM_s} J_s. \tag{6}$$

The spin-dependent Seebeck effect will drive a pure spin current with equal numbers of spin-↑ and spin-↓ electrons moving in opposite directions, that is to say, $J_\uparrow = -J_\downarrow$, ensuring that the net charge current $J_e = J_\uparrow + J_\downarrow = 0$, as required by the open circuit configuration of our experiment. Meanwhile, $J_s = J_\uparrow - J_\downarrow$.

To determine the electronic spin current we use the expression given by Yi *et al.* [24]

$$J_s = -\frac{2\sigma_\uparrow \sigma_\downarrow}{\sigma_\uparrow + \sigma_\downarrow}(S_\uparrow - S_\downarrow)\nabla T, \tag{7}$$

where $\sigma_{\uparrow,\downarrow}$ are the spin-resolved electrical conductivities and $S_{\uparrow,\downarrow}$ are the spin-resolved Seebeck coefficients. We can obtain the spin-resolved conductivities from knowledge of the resistivity of a material (here we use the value $\rho = 21\ \mu\Omega\,\mathrm{cm}$ measured for our multilayer as a whole and assume that the magnetic layers have this stack-averaged resistivity) combined with a value for P. Using a rough estimate for $P = 0.5$, we obtain

$$\sigma_\uparrow = \frac{1+P}{2\rho} = 3.6 \times 10^6\,\Omega^{-1}\,\mathrm{m}^{-1}, \tag{8a}$$

$$\sigma_\downarrow = \frac{1-P}{2\rho} = 1.2 \times 10^6\,\Omega^{-1}\,\mathrm{m}^{-1}. \tag{8b}$$

The spin-dependent Seebeck coefficients of CoB are unknown. As an upper limit, we use the values for Co obtained in the experiments of Yang *et al.* [46], $S_\uparrow = -2$ μV/K and $S_\downarrow = -73$ μV/K. Inserting all these values in Eq. (S7), for a gradient of -20 K/μm, we obtain a pure spin current of $J_s = 2.5\,\mathrm{GA/m^2}$.

Taking the same values for α, β, and M_s as for the spin Seebeck magnon currents, we obtain, from Eq. (6), $v = -27$ cm/s. Again, the sign of the effect matches the observed motion, although we still have the same discrepancy in magnitude between the creep and viscous flow regimes. Although for these parameters the effect is a few times stronger than that arising from the magnon current, the real value could be less, given that we do not know well the values of parameters such as P and $S_\uparrow$ and $S_\uparrow$ in such thin magnetic layers.

C. Energy gradients

The domain wall velocity due to gradients in the micromagnetic free energy parameters can be derived from the Landau-Lifshitz-Bloch equation [26]. Below the Walker breakdown, the velocity is

$$v = \frac{\gamma}{\alpha M_0}\left[1 + \alpha^2\left(\frac{M_0}{M_s}\right)^2\right]\left(\frac{M_s B_z \Delta}{\pi} - 2\frac{\partial A}{\partial x}\right). \tag{9}$$

$\Delta = \sqrt{A/K}$ is the domain wall width. In our experiments the domains do not move with an applied field, so we neglect the field term in this equation, leaving

$$v = -\frac{2\gamma}{\alpha M_0}\left[1 + \alpha^2\left(\frac{M_0}{M_s}\right)^2\right]\frac{\partial A}{\partial x}. \tag{10}$$

The derivative of the spatial dependence of the exchange stiffness can be related to the temperature gradient through the chain rule

$$\frac{\partial A}{\partial x} = \frac{\partial A}{\partial T}\frac{\partial T}{\partial x}. \tag{11}$$

To obtain $\partial A/\partial T$, we need the temperature dependence of A. It is often written as a power law in the reduced magnetization $A(T) = A_0(M_s/M_0)^\alpha$, where $\alpha = 2$ in the mean field picture [47]. However, this result is derived for classical Rayleigh-Jeans statistics rather than Planck statistics that are already

assumed within Bloch's law and therefore M_s. To have a consistent approach, we therefore calculate the temperature dependence of A from the temperature dependence of the spin wave stiffness [48],

$$D(T) = D_0\left(1 - \frac{U_T}{2U_0}\right), \tag{12}$$

where $U_0 = 3D_0M_0/(\hbar\gamma\delta^2)$ is the energy density per spin, with δ being the nearest-neighbor distance between atoms, and $U(T)$ is the energy density of the magnon gas at temperature T. The exchange stiffness is related to the spin wave stiffness by

$$A(T) = \frac{M_s}{2\hbar\gamma}D(T). \tag{13}$$

By the product rule, we obtain

$$\frac{\partial A}{\partial T} = \frac{1}{2\hbar\gamma}\left(M_s\frac{\partial D}{\partial T} + \frac{\partial M_s}{\partial T}D\right). \tag{14}$$

For the very thin films in these experiments, Bloch's law in the usual "bulk" form cannot be used [49–51]. The quantization of the spin waves in the thin direction leads to significant differences in the equations and the value of stiffness extracted from experiments. The thin film form of Bloch's law is

$$M_s(T) = M_0 + \frac{\gamma\hbar}{4\pi L_z}\frac{k_BT}{D_0}\sum_{m=0}^{N-1}\ln\left[1 - \exp\left(-\frac{\omega_m}{k_BT}\right)\right], \tag{15}$$

where L_z is the thickness of the thin film, N is the number of atomic planes within that thickness and

$$\omega_m = \gamma\hbar B_z - D_0\left(\frac{m\pi}{(N-1)a}\right)^2. \tag{16}$$

This expression is cumbersome to take derivatives of, so we approximate the zeroth term of the sum using $\ln[1 - \exp(-x)] \approx \ln x$ as $x \to 0^+$ and using the fact that N is a small number such that the first term of the summation is the dominant term and use the series expansion $\ln(1 - e^{-x}) = -\sum_{n=1}^{\infty} e^{-nx}/n$. Our approximate form is

$$M_s(T) \approx M_0 + \frac{\gamma\hbar}{4\pi L_z}\frac{k_BT}{D_0}\left[\ln\frac{\omega_0}{k_BT} - \exp\left(-\frac{\omega_1}{k_BT}\right)\right]. \tag{17}$$

The derivative is then

$$\frac{\partial M_s}{\partial T} \approx \frac{\gamma\hbar k_B}{4\pi L_zD_0}\left[\ln\left(\frac{\omega_0}{k_BT}\right) - \exp\left(-\frac{\omega_1}{k_BT}\right) - \frac{\omega_1}{k_BT}\exp\left(-\frac{\omega_1}{k_BT}\right) - 1\right]. \tag{18}$$

We can similarly derive an expression for the internal energy density of the magnon gas in a thin film, finding

$$U(T) = \frac{(k_BT)^2}{4\pi L_zD_0}\sum_{m=0}^{N-1}\mathrm{Li}_2\left[\exp\left(-\frac{\omega_m}{k_BT}\right)\right] - \frac{\omega_m}{k_BT}\ln\left[1 - \exp\left(-\frac{\omega_m}{k_BT}\right)\right], \tag{19}$$

where $\mathrm{Li}_2(x)$ is the dilogarithm function. Again, we look to approximate this and write an expression that contains only ω_0 and ω_1:

$$U(T) \approx \frac{(k_BT)^2}{4\pi L_zD_0}\left\{\mathrm{Li}_2\left[\exp\left(-\frac{\omega_0}{k_BT}\right)\right] + \mathrm{Li}_2\left[\exp\left(-\frac{\omega_1}{k_BT}\right)\right] - \frac{\omega_1}{k_BT}\ln\left[1 - \exp\left(-\frac{\omega_1}{k_BT}\right)\right]\right\}, \tag{20}$$

which is a reasonable approximation within the low-temperature limits of Bloch's law. The derivative of this expression is

$$\begin{aligned}\frac{\partial U}{\partial T} \approx \frac{k_B^2T}{2\pi L_zD_0}\Bigg\{&\mathrm{Li}_2\left[\exp\left(-\frac{\omega_0}{k_BT}\right)\right] - \frac{\omega_0}{2k_BT}\ln\left[1 - \exp\left(-\frac{\omega_0}{k_BT}\right)\right]\\ &+ \mathrm{Li}_2\left[\exp\left(-\frac{\omega_1}{k_BT}\right)\right] - \frac{\omega_1}{k_BT}\ln\left[1 - \exp\left(-\frac{\omega_1}{k_BT}\right)\right] + \frac{\omega_1^2}{2(k_BT)^2}\frac{1}{\exp\left(-\frac{\omega_1}{k_BT}\right) - 1}\Bigg\}.\end{aligned} \tag{21}$$

Using the values $M_0 = 803$ kA/m, $D_0 = 5.65 \times 10^{-40}$ J m^2 (from our fit to Bloch's law in [38]), $\delta = 2.51$ Å, $B_z = 30$ Oe, $L_z = 0.8$ nm, and $N = 4$ in Eq. (10), we find $v = -112$ cm/s. This is substantially larger than the viscous flow velocities obtained from either of the magnonic or electronic STTs and thus can be expected to be the predominant mechanism causing the motion of the domains up the temperature gradient toward the heater. Indeed, the two STT-based mechanisms appear to be too weak even to be able to overcome the threshold for domain motion for the range of temperature gradients in this study.

IV. CONCLUSION

To summarize, the displacement of reverse domains in a perpendicularly magnetized metallic multilayer driven by a temperature gradient was observed by MFM. The domains always move toward the hotter region. By canceling the effect of Oersted fields generated by the calibrated thermometer and heater wire we were able to quantify the effect: We saw velocities of ∼1 nm/s under a temperature gradient of ∼20 K/μm, slow enough to be in the creep regime. By estimating the relative size of different possible driving mechanisms

based on the experimentally measured properties of our multilayer we found that the entropic forces [26] are expected to predominate, confirming Landau-Lifshitz-Bloch-based simulations [28]. Cleverly engineering the temperature dependence of the DW energy, e.g., using layers with phase transitions at controlled temperatures or novel scaling relations between micromagnetic parameters, could allow these currently quite weak entropic forces to become large enough to be useful, perhaps operating using scavenged waste heat.

ACKNOWLEDGMENTS

We wish to thank Philippa Shepley, Nathan Satchell, and Md Golam Hafiz for their experimental assistance.

DATA AVAILABILITY

The data that support the findings of this article are openly available [52].

[1] G. E. W. Bauer, E. Saitoh, and B. J. van Wees, Spin caloritronics, Nat. Mater. **11**, 391 (2012).

[2] H. Adachi, K.-I. Uchida, E. Saitoh, and S. Maekawa, Theory of the spin Seebeck effect, Rep. Prog. Phys. **76**, 036501 (2013).

[3] H. Yu, S. D. Brechet, and J.-P. Ansermet, Spin caloritronics, origin and outlook, Phys. Lett. A **381**, 825 (2017).

[4] K.-I. Uchida, Transport phenomena in spin caloritronics, Proc. Jpn. Acad., Ser. B **97**, 69 (2021).

[5] C. H. Marrows, Spin-polarised currents and magnetic domain walls, Adv. Phys. **54**, 585 (2005).

[6] D. C. Ralph and M. D. Stiles, Spin transfer torques, J. Magn. Magn. Mater. **320**, 1190 (2008).

[7] A. Thiaville, S. Rohart, E. Jué, V. Cros, and A. Fert, Dynamics of Dzyaloshinskii domain walls in ultrathin magnetic films, Europhys. Lett. **100**, 57002 (2012).

[8] F. Jonietz, S. Mühlbauer, C. Pfleiderer, A. Neubauer, W. Münzer, A. Bauer, T. Adams, R. Georgii, P. Böni, R. A. Duine, K. Everschor, M. Garst, and A. Rosch, Spin transfer torques in MnSi at ultralow current densities, Science **330**, 1648 (2010).

[9] W. Jiang, P. Upadhyaya, W. Zhang, G. Yu, M. B. Jungfleisch, F. Y. Fradin, J. E. Pearson, Y. Tserkovnyak, K. L. Wang, O. Heinonen, S. G. E. te Velthuis, and A. Hoffmann, Blowing magnetic skyrmion bubbles, Science **349**, 283 (2015).

[10] S. Woo, K. Litzius, B. Krüger, M.-Y. Im, L. Caretta, K. Richter, M. Mann, A. Krone, R. M. Reeve, M. Weigand, P. Agrawal, I. Lemesh, M.-A. Mawass, P. Fischer, M. Kläui, and G. S. D. Beach, Observation of room-temperature magnetic skyrmions and their current-driven dynamics in ultrathin metallic ferromagnets, Nat. Mater. **15**, 501 (2016).

[11] K. Zeissler, S. Finizio, C. Barton, A. J. Huxtable, J. Massey, J. Raabe, A. V. Sadovnikov, S. A. Nikitov, R. Brearton, T. Hesjedal, G. van der Laan, M. C. Rosamond, E. H. Linfield, G. Burnell, and C. H. Marrows, Diameter-independent skyrmion Hall angle observed in chiral magnetic multilayers, Nat. Commun. **11**, 428 (2020).

[12] K. Uchida, J. Xiao, H. Adachi, J. Ohe, S. Takahashi, J. Ieda, T. Ota, Y. Kajiwara, H. Umezawa, H. Kawai, G. E. W. Bauer, S. Maekawa, and E. Saitoh, Spin Seebeck insulator, Nat. Mater. **9**, 894 (2010).

[13] C. M. Jaworski, J. Yang, S. Mack, D. D. Awschalom, J. P. Heremans, and R. C. Myers, Observation of the spin-Seebeck effect in a ferromagnetic semiconductor, Nat. Mater. **9**, 898 (2010).

[14] K. Uchida, M. Ishida, T. Kikkawa, A. Kirihara, T. Murakami, and E. Saitoh, Longitudinal spin Seebeck effect: From fundamentals to applications, J. Phys. Condens. Matter **26**, 343202 (2014).

[15] A. A. Kovalev and Y. Tserkovnyak, Thermoelectric spin transfer in textured magnets, Phys. Rev. B **80**, 100408(R) (2009).

[16] J. C. Slonczewski, Initiation of spin-transfer torque by thermal transport from magnons, Phys. Rev. B **82**, 054403 (2010).

[17] D. Hinzke and U. Nowak, Domain wall motion by the magnonic spin Seebeck effect, Phys. Rev. Lett. **107**, 027205 (2011).

[18] P. Yan, X. S. Wang, and X. R. Wang, All-magnonic spin-transfer torque and domain wall propagation, Phys. Rev. Lett. **107**, 177207 (2011).

[19] X.-G. Wang, G.-H. Guo, Y.-Z. Nie, G.-F. Zhang, and Z.-X. Li, Domain wall motion induced by the magnonic spin current, Phys. Rev. B **86**, 054445 (2012).

[20] A. A. Kovalev and Y. Tserkovnyak, Thermomagnonic spin transfer and Peltier effects in insulating magnets, Europhys. Lett. **97**, 67002 (2012).

[21] P. Yan, Y. Cao, and J. Sinova, Thermodynamic magnon recoil for domain wall motion, Phys. Rev. B **92**, 100408(R) (2015).

[22] M. A. S. Akanda, M. T. Islam, and X. R. Wang, Role of SSW on thermal-gradient induced domain-wall dynamics, J. Phys. Condens. Matter **35**, 315701 (2023).

[23] K. Uchida, S. Takahashi, K. Harii, J. Ieda, W. Koshibae, K. Ando, S. Maekawa, and E. Saitoh, Observation of the spin Seebeck effect, Nature (London) **455**, 778 (2008).

[24] L. Yi, D. Yang, M. Liu, H. Fu, L. Ding, Y. Xu, B. Zhang, L. Pan, and J. Q. Xiao, Concepts of spin Seebeck effect in ferromagnetic metals, Adv. Funct. Mater. **30**, 2004024 (2020).

[25] Y.-R. Wang, C. Yang, Z.-C. Wang, and G. Su, Domain-wall dynamics driven by thermal and electrical spin-transfer torque, Phys. Rev. B **106**, 054432 (2022).

[26] F. Schlickeiser, U. Ritzmann, D. Hinzke, and U. Nowak, Role of entropy in domain wall motion in thermal gradients, Phys. Rev. Lett. **113**, 097201 (2014).

[27] J. Chico, C. Etz, L. Bergqvist, O. Eriksson, J. Fransson, A. Delin, and A. Bergman, Thermally driven domain-wall motion in Fe on W(110), Phys. Rev. B **90**, 014434 (2014).

[28] S. Moretti, V. Raposo, E. Martinez, and L. Lopez-Diaz, Domain wall motion by localized temperature gradients, Phys. Rev. B **95**, 064419 (2017).

[29] H. Yu, S. Granville, D. P. Yu, and J.-P. Ansermet, Evidence for thermal spin-transfer torque, Phys. Rev. Lett. **104**, 146601 (2010).

[30] P. Möhrke, J. Rhensius, J.-U. Thiele, L. Heyderman, and M. Kläui, Tailoring laser-induced domain wall pinning, Solid State Commun. **150**, 489 (2010).

[31] J. P. Tetienne, T. Hingant, J.-V. Kim, L. H. Diez, J.-P. Adam, K. Garcia, J. F. Roch, S. Rohart, A. Thiaville, D. Ravelosona, and V. Jacques, Nanoscale imaging and control of domain-wall

hopping with a nitrogen-vacancy center microscope, Science **344**, 1366 (2014).

[32] A. J. Ramsay, P. E. Roy, J. A. Haigh, R. M. Otxoa, A. C. Irvine, T. Janda, R. P. Campion, B. L. Gallagher, and J. Wunderlich, Optical spin-transfer-torque-driven domain-wall motion in a ferromagnetic semiconductor, Phys. Rev. Lett. **114**, 067202 (2015).

[33] W. Jiang, P. Upadhyaya, Y. Fan, J. Zhao, M. Wang, L.-T. Chang, M. Lang, K. L. Wong, M. Lewis, Y.-T. Lin, J. Tang, S. Cherepov, X. Zhou, Y. Tserkovnyak, R. N. Schwartz, and K. L. Wang, Direct imaging of thermally driven domain wall motion in magnetic insulators, Phys. Rev. Lett. **110**, 177202 (2013).

[34] J. Torrejon, G. Malinowski, M. Pelloux, R. Weil, A. Thiaville, J. Curiale, D. Lacour, F. Montaigne, and M. Hehn, Unidirectional thermal effects in current-induced domain wall motion, Phys. Rev. Lett. **109**, 106601 (2012).

[35] X. Yu, *et al.*, Real-space observations of 60-nm skyrmion dynamics in an insulating magnet under low heat flow, Nat. Commun. **12**, 5079 (2021).

[36] Z. Wang, *et al.*, Thermal generation, manipulation and thermoelectric detection of skyrmions, Nat. Electron. **3**, 672 (2020).

[37] E. Raimondo, E. Saugar, J. Barker, D. Rodrigues, A. Giordano, M. Carpentieri, W. Jiang, O. Chubykalo-Fesenko, R. Tomasello, and G. Finocchio, Temperature-gradient-driven magnetic skyrmion motion, Phys. Rev. Appl. **18**, 024062 (2022).

[38] See Supplemental Material at http://link.aps.org/supplemental/10.1103/152r-5wvt for further details of the sample fabrication and characterisation as well as details of the data analysis.

[39] D. Nečas and P. Klapetek, Gwyddion: An open-source software for SPM data analysis, Cent. Eur. J. Phys. **10**, 181 (2012).

[40] P. Kienzle, J. Krycka, N. Patel, and I. Sahin, bumps, version 0.9.2, https://pypi.org/project/bumps/.

[41] P. J. Metaxas, J. P. Jamet, A. Mougin, M. Cormier, J. Ferré, V. Baltz, B. Rodmacq, B. Dieny, and R. L. Stamps, Creep and flow regimes of magnetic domain-wall motion in ultrathin Pt/Co/Pt films with perpendicular anisotropy, Phys. Rev. Lett. **99**, 217208 (2007).

[42] A. A. Thiele, Steady-state motion of magnetic domains, Phys. Rev. Lett. **30**, 230 (1973).

[43] A. Thiaville, Y. Nakatani, J. Miltat, and Y. Suzuki, Micromagnetic understanding of current-driven domain wall motion in patterned nanowires, Europhys. Lett. **69**, 990 (2005).

[44] L. J. Cornelissen, K. J. H. Peters, G. E. W. Bauer, R. A. Duine, and B. J. van Wees, Magnon spin transport driven by the magnon chemical potential in a magnetic insulator, Phys. Rev. B **94**, 014412 (2016).

[45] J Bass and W. Pratt, Current-perpendicular (CPP) magnetoresistance in magnetic metallic multilayers, J. Magn. Magn. Mater. **200**, 274 (1999).

[46] D. Yang, L. Yi, S. Fan, X. He, Y. Xu, M. Liu, L. Ding, L. Pan, and J. Q. Xiao, Spin Seebeck coefficients of Fe, Co, Ni, and $Ni_{80}Fe_{20}$ 3d-metallic thin films, Mater. Res. Bull. **136**, 111153 (2021).

[47] U. Atxitia, D. Hinzke, O. Chubykalo-Fesenko, U. Nowak, H. Kachkachi, O. N. Mryasov, R. F. Evans, and R. W. Chantrell, Multiscale modeling of magnetic materials: Temperature dependence of the exchange stiffness, Phys. Rev. B **82**, 134440 (2010).

[48] C. Kittel, *Quantum Theory of Solids* (Wiley, New York, 1963).

[49] H. T. Nembach, J. M. Shaw, M. Weiler, E. Jué, and T. J. Silva, Linear relation between Heisenberg exchange and interfacial Dzyaloshinskii–Moriya interaction in metal films, Nat. Phys. **11**, 825 (2015).

[50] J. B. Mohammadi, B. Kardasz, G. Wolf, Y. Chen, M. Pinarbasi, and A. D. Kent, Reduced exchange interactions in magnetic tunnel junction free layers with insertion layers, ACS Appl. Electron. Mater. **1**, 2025 (2019).

[51] K. Alshammari, E. Haltz, M. Alyami, M. Ali, P. S. Keatley, C. H. Marrows, J. Barker, and T. A. Moore, Scaling of Dzyaloshinskii-Moriya interaction with magnetization in Pt/Co(Fe)B/Ir multilayers, Phys. Rev. B **104**, 224402 (2021).

[52] L. Huang, J. Barker, L. Kailas, S. D. Connell, G. Burnell, and C. H. Marrows, Data associated with "Temperature gradient driven motion of magnetic domains in a magnetic metal multilayer by entropic forces", Research Data Leeds (2025), https://doi.org/10.5518/1796.